2013 IEEE/RSJ International Conference on
Intelligent Robots and Systems (IROS)
November 3-7, 2013. Tokyo, Japan

Design Evaluation of a Double Ring RCM Mechanism for Robotic Needle Guidance in MRI-guided Liver Interventions

Sang-Eun Song, Junichi Tokuda, Kemal Tuncali, Atsushi Yamada, Meysam Torabi, and Nobuhiko Hata

Abstract— **MRI-guided percutaneous liver interventions have been investigated by researchers as an alternative to CT-guided procedures as it is non-invasive and provides greater soft tissue details. In practice, however, repeated needle insertion is still required to reach desired positions on trial-and-error basis. To minimize the needle attempt and procedural time, we designed a robotic needle guidance device that provides needle insertion angle guidance at skin entry using two rotational joints structured for remote-center-of-motion manipulation. To evaluate the mechanism and clinical feasibility, we fabricated a proof-of-concept prototype that can be manually operated. As preliminary design evaluation, we conducted a retrospective clinical study of 13 MRI-guided abdominal biopsies to determine if the proposed mechanism and device can provide necessary needle insertion angles in MRI-guided liver biopsy procedures. The number of needle insertion attempts per biopsy was also measured. To confirm the kinematic design of the double ring remote-center-of-motion mechanism and to identify any procedural difficulties, we conducted a phantom targeting experiment. The retrospective clinical study showed that the 80 degree insertion angle coverage of the device is sufficient for clinical cases, and an average of five needle insertion attempts per biopsy in conventional MRI-guided biopsy can be reduced by the proposed device. A phantom targeting experiment confirmed that the unique kinematic design was successfully implementation in the targeting.**

I. Introduction

Magnetic Resonance Imaging (MRI) has exhibited excellent spatial resolution, superior soft tissue contrast and multiparametric imaging capability. The usage of MR images in guidance of interventional tools has demonstrated its potential and effectiveness in various interventional procedures including neurosurgery [2], ablation treatment [3], and prostate therapy [4, 5]. This growing technology has also been overcoming associated technical challenges, including slow image acquisition which takes a few seconds up to minutes and consequently defects the interactiveness between the needle steering and patient imaging [6].

Another crucial issue takes place where the clinician does not have the direct access to the patient due to the limited space within closed-bore MR scanners. Open-bore scanners are also available but would not be an ultimate solution for such a problem since they degrade the image quality [7]. As a result, robotic approaches have been proposed by researchers and are being pursued in order to operate inside the bore without having to move the patient inside and outside the bore repeatedly for imaging and intervention.

Since conventional electrical motors are not suitable to be used in the high magnetic fields, such MRI-compatible robotic systems are actuated by either pneumatic actuators [7-9] or piezoelectric motors [6, 10, 11]. Although the MR field imposes significant constraints for actuator and material selection, it has also shown benefits such as powering and driving actuators using the magnetic field [12, 13].

MRI-guided percutaneous liver interventions are one of the clinical applications that can benefit from MRI-compatible robotic assistant since precisely placing a needle at a target position with MR images is a time consuming task for clinicians. Moreover, the trial-and-error based needle insertion may increase the risk of damaging important anatomical features such as organs and blood vessels, which are visible in MRI.

At Brigham and Women's Hospital, clinicians have been performing MRI-guided liver interventions to utilize the advantages of MRI. Although the new procedures have already provided greater diagnostic and therapeutic utilities, researcher have also been investigating an MRI-compatible robotic assistant that can minimize the aforementioned limitations to deliver further optimized interventions.

Based on the design requirements identified from the current clinical environment and literature, we designed an MRI-compatible robotic needle insertion device for MRI-guided liver interventions using a double ring remote-center-of-motion (RCM) mechanism to deliver needle insertion via single skin entry. We also developed a 3D Slicer (http://www.slicer.org) module that provides planning and navigation.

As a proof-of-concept model, we designed and fabricated a rapid prototype model that can provide needle insertion angle manually using the double ring mechanism. In this paper, we introduce the details of a manual device and its kinematics. We also report a retrospective clinical study for clinical feasibility evaluation, and a phantom experiment to evaluate the protocol and identify unforeseen problems.

This project was supported by Canon Inc.

S. Song*, J. Tokuda, A. Yamada, M. Torabi and N. Hata are with the Surgical Navigation and Robotics Laboratory at the Department of Radiology, Brigham and Women's Hospital, Harvard Medical School, Boston, MA 02115 USA (email: {sam, tokuda, ayamada, torabi, hata}@bwh.harvard.edu). K. Tuncali is with the Department of Radiology, Brigham and Women's Hospital, Harvard Medical School, Boston, MA 02115 USA (email: ktuncali @partners.org).

* Corresponding author (phone: 617-732- 5059; fax: 617-582-6033).

II. Robotic Needle Insertion

A. Design Approach

We designed an MRI-compatible robotic device that can perform needle placement for core needle biopsy, RF ablation and cryotherapy in the abdominal organs e.g. liver and kidney for accurate needle placement taking advantage of superior tumor detection capability of modern MR imaging technologies. The device can guide the needle in a strong magnetic field up to 3T as well as RF electromagnetic field used for MR imaging without interfering magnetic resonance signal detection for image reconstruction.

Our hypothesis is that an MRI-compatible device that works during imaging allows remotely-controlled needle insertion using real-time image feedback, thus it can achieve more accurate needle placement and shorter operating time than the current practice of manual MRI-guided interventions, where a patient is moved outside of the scanner for needle placement and moved back inside the scanner for confirmation imaging.

The device consists of linear needle insertion driver and novel 2-DOF needle orientation mechanism shown in Fig. 1 (A). The device can be attached to the patient table of the MRI scanner using a lockable positioning arm. The device then can be located at the needle entry point of the patient's abdominal wall. Alternatively, the device can be attached on skin, which is similar to the patient-mounted approach, proposed by Walsh et al. for CT-guided tele-robotic tool for percutaneous interventions [14].

B. Requirements and Kinematics

The preliminary requirements for the needle insertion mechanism are shown in Table 1. The needle orientation mechanism allows angling the needle with remote-center-of-motion at the needle entry point on the skin. The proposed needle angling mechanism has primarily two advantages over other devices proposed by other researchers. First, the mechanism can be compact enough to be operated inside a gantry of MRI scanner. Second, the mechanism does not have any joint, which usually compromises rigidity of the structure. Therefore, it potentially improves the accuracy of needle placement.

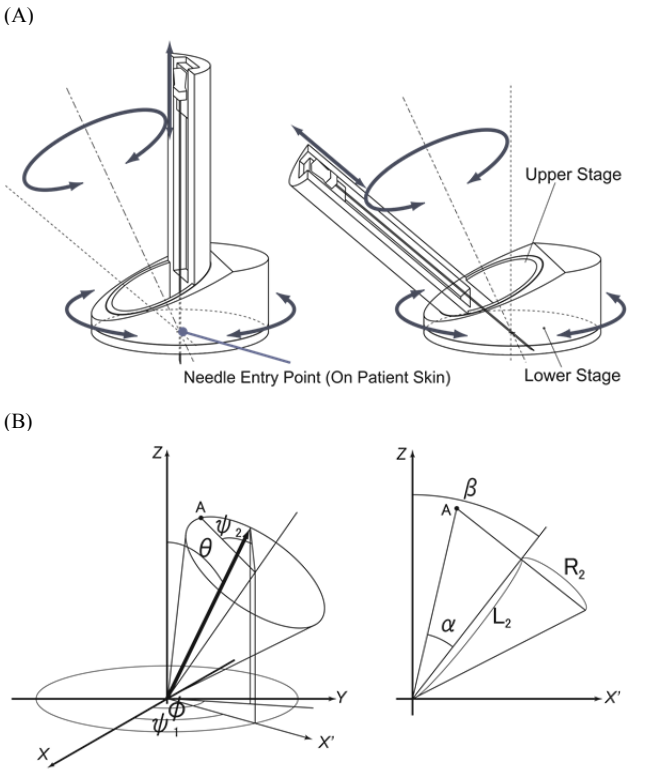

Figure 1. (A) Concept of needle orientation and insertion mechanism. The needle at vertical orientation and at maximum tilt are shown. (B) Definitions of angle parameters to control needle orientation. The mechanism consists of two rotational and one translational degree-of-freedom.

The needle orientation mechanism consists of upper and lower rotary stages with angle of 20 degrees between two rotation axes. Rotation of each stage can be achieved by ring-type piezoelectric motors or it can be achieved via flexible shafts rotated by the clinician standing outside the scanner in case of manual manipulation. The shafts can also be driven by non-magnetic piezoelectric actuators for an automated manipulation. The needle driver is attached to the upper stage with a 20 degrees angulation from the axis of stage. Given the coordinate system fixed to the base of the lower stage as shown in Fig. 1 (B) and rotation angles of the lower stage ψ_1 and the upper stage ψ_2, the angle θ and φ in the figure (as defined in the polar coordinate system) can be

TABLE 1. Requirements for the needle insertion mechanism and controller

Requirement	Value	Description
Width	< 200 mm	Based on workspace analysis in scanner with 70cm bore
Depth	< 200 mm	Based on workspace analysis in scanner with 70cm bore
Height (incl. needle)	< 150 mm	Based on workspace analysis in scanner with 70cm bore
Targeting error	< 3 mm	Based on minimum tumor size and interview with an interventional radiologist
Needle tilting angle	> 40 deg	Assuming the angle between skin surface and needle is more than 20 deg.
Needle tilting speed	40 deg/s	Maximum angle range divided by duration for needle tilting

described as:

$$\varphi = \psi_1 + \varphi$$
$$\theta = \theta' \quad (1)$$

where,

$$\cos\varphi' = \frac{\sin\beta - \tan\alpha\cos\psi_2\cos\beta}{\sqrt{(\sin\beta - \tan\alpha\cos\psi_2\cos\beta)^2 + \tan^2\alpha\sin^2\psi_2}}$$
$$\sin\varphi' = \frac{\tan\alpha\sin\psi_2}{\sqrt{(\sin\beta - \tan\alpha\cos\psi_2\cos\beta)^2 + \tan^2\alpha\sin^2\psi_2}} \quad (2)$$
$$\cos\theta' = \frac{\cos\alpha\cos\beta}{L_2}$$

By calculating the inverse kinematics, a set of ψ_1 and ψ_2 that gives desired θ and φ can be determined. This can be implemented in the targeting software, which displays the appropriate dial position to obtain the needle orientation aligned to the target, based on the current position of the device and the target position.

To calculate the appropriate dial position to obtain the needle orientation aligned to the target based on the current position of the target in the MR image space, the targeting software must register the device coordinate system to the MR image coordinate system. This can be achieved by a fiducial-based registration method using a Z-frame [15] that has been developed and clinically used in our previous study on a MRI-compatible manipulator for prostate intervention [11].

The Z-frame or other design of MR-visible registration marker set can be attached or embedded to the base of needle orientation and insertion device. Any arbitrary MR image slicing through the registration markers provides the full 6 DOF pose of the frame, and hence the robot, with respect to the scanner. Thus, by locating the fiducial attached to the needle orientation and insertion device, the transformation between image coordinate and the robot coordinate is identified.

III. Manual Device Development

A. Proof-of-Concept Model

In order for rapid clinical implementation, a manually driven device has been selected as an initial development step. To investigate the feasibility of the device mechanism and its clinical protocol adaptability, we designed and fabricated a rapid prototype model of the manual device for single needle insertion in MRI-guided liver interventions shown in Fig. 2. The device is skin-attached and can accommodate a 110 mm diameter Loop coil and Body Matrix coil (Siemens Healthcare, Erlangen, Germany) in the base area**.**

The manual device we developed consists of two active rings. The lower larger ring is on the base and the other smaller ring is located onto the larger ring in 20 degree slanted angle. This unique structure enables the needle to pivot on a RCM at the center of lower surface of the base. Therefore,

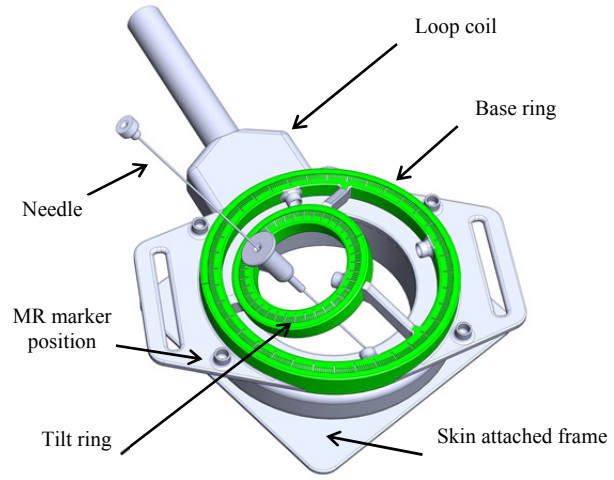

Figure 2. CAD model of a proof-of-concept model with a loop-shaped imaging coil.

once a target position is identified, the needle path can be calculated and provided by rotating the base ring and the tilted ring accordingly, which is calculated by the navigation software.

Regarding the in-bore space limitation, the height of the device is approximately 8 cm. With an average size of patients' chest thickness, the device structure with a partially inserted needle would not exceed the internal diameter of the 70 cm diameter closed bore. With the skin-attached design, patient's respiratory motions could be, in part, cancelled out, since the robot and chest move simultaneously.

Since the robot is very close to the imaging coil, it may introduce image degradation. However, literature shows that piezoelectric actuators, which we use to drive the robot, have a minimal noise, an average signal-to-noise-ratio (SNR) loss of less than 2% in magnetic fields [16], and the MR images, obtained while motors operating, are medically acceptable [3].

B. Targeting Kinematics

The inverse kinematics for this unique structure was given as follows based on a schematic diagram of Fig. 3. Let

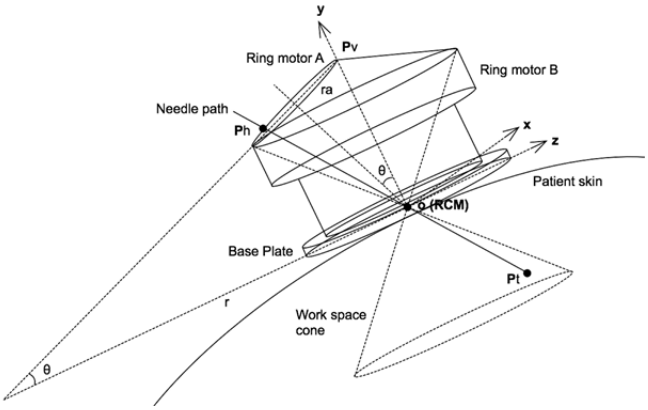

Figure 3. A dimensional schematic model of the manual needle guidance device for MRI-guided liver intervention.

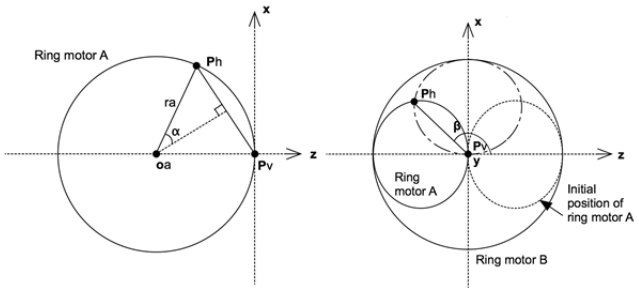

Figure 4. (A) Structure diagram of the ring motor A. o_a and r_a are the center of the ring and the radius, respectively. p_v is the initial position of the needle holder and p_h is the point of intersection of planned needle path and the surface of the ring motor A. (B) Two-ring structure diagram. p_v is the initial position of the needle holder and p_h is the point of intersection of planned needle path and the surface of the ring motor A. A solid line of ring motor A represents the position to realize the planned needle path. The dashed line represents an alternative solution of the position of the ring motor A. The dotted line represents an initial position of the ring motor A.

$p := [x\ y\ z] \in R^3$ and $p_t := [x_t\ y_t\ z_t] \in R^3$ be any position on a needle path and a target position, respectively. The location of the RCM is the origin. Since the needle path always goes through the RCM, the needle path is given as a line as follows:

$$p = p_t t \tag{3}$$

where t is a parameter and p_t acts as an direction vector.

Let $p_h := [x_h\ y_h\ z_h] \in R^3$ and $p_v := [0\ k\ 0] \in R^3$ be the position of the needle holder and its initial position, respectively. p_v represents the vertex coordinate of the cone and k is a design parameter. The location of the needle holder p_h draws a right circular cone by the mechanical constraints when both rings are rotated as shown in Fig. 3. Therefore, the location of the holder to realize needle path to reach the target position can be obtained from simultaneous equations for Eq. (3) and the following surface equation of the circular cone:

$$k^2(x^2 + z^2) = r^2(y - k)^2 \tag{4}$$

where r is the radius of the cone. From the fact that $k = r\ tan\,\theta$, the location of needle holder p_h is given as follows:

$$p_h = p_t\ t_h \tag{5}$$

where t_h is the following line parameter:

$$t_h = \frac{r\tan\theta\left\{y_t - \sqrt{2y_t{}^2 - \tan{}^2\theta(x_t^2 + z_t^2)}\right\}}{(\tan{}^2\theta)(x_t^2 + z_t^2) - y_t^2} \tag{6}$$

Once the position of p_h is obtained, one can calculate the rotational angle of the tilted ring θ_{tilt} by using a geometry of an isosceles triangle as shown in Fig. 4 (A).

$$\theta_{tilt} = 2\alpha = 2\sin^{-1}\left(\frac{|p_h - p_v|}{2r_a}\right) \tag{7}$$

where r_a is the radius of the ring. The initial position of the tilted ring is shown in Fig. 4 (B). Therefore, the rotational angle of the base ring θ_{base} is given to place the needle holder at p_h as follows:

$$\theta_{base} = \text{sign}(x_h)\beta + \frac{\pi}{2} - \alpha \tag{8}$$

Where $\text{sign}(x_h)$ represents a sign of x_h, β is the angle between z-axis of positive side and the projected line of $p_h p_v$ to xz plane as follows:

$$\beta = \cos^{-1}\frac{z_h}{x_h^2 + z_h^2} \tag{9}$$

The specification of the needle assist device is summarized in Table 2. The workspace of the needle assist device is formed as a cone shape and the angle of the cone is determined by the tilted angle in Table 2 also shown in Fig 3. The height of the workspace depends on the length of the needle and the required needle length d_n can be calculated by using the geometric constraint for the device as follows:

$$d_n = |p_v - p_t| \tag{10}$$

TABLE 2. DESIGN PARAMETERS OF MANUAL NEEDLE GUIDANCE DEVICE

Description	Variable	Value	Unit
Vertex coordinate of the device	k	61.3	mm
Tilted angle of small ring	θ	20.0	deg
Radius for tilted ring	r_a	22.50	mm
Workspace cone angle	4θ	80.0	deg

The software for point based registration, identifying target positions and planning needle path has been developed and implemented as a module in the open-source visualization and navigation software 3D Slicer. This module provides features for planning and managing a target for liver ablation and biopsy. The software provides point to point registration to register the device coordinate to the image coordinate. Then, users can place a target point to define the target location on intraprocedural MRI volume loaded into 3D Slicer. Fig. 5 illustrates the device positioning sequence.

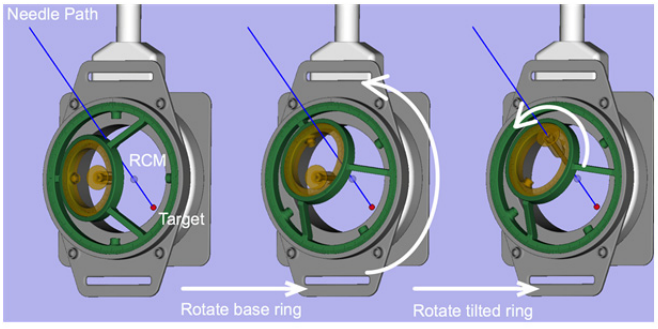

Figure 5. Needle guidance sequence: once a target is identified, a needle path that includes the target and RCM is created. Then, required rotation values for two rings are computed from the needle path. First, the larger base ring rotates to the calculated position followed by the smaller ring.

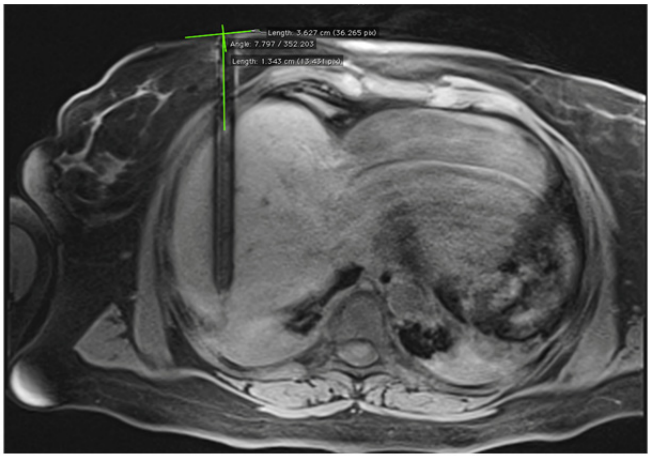

Figure 6. A representitive image of the restrospective clinical study showing needle artifact and possible device attachement angle. The line tangential to the skin represents the skin attachement line.

IV. Retrospective Clinical Study

A. Method and Data Acquisition

To evaluate the device design and approach, a retrospective clinical study has been conducted. The study was approved by the institutional review board (IRB) at Brigham and Women's Hospital and is HIPPA compliant. The study includes 13 image datasets of 12 patients (age 38-81 years; 7 men and 5 women) who underwent MRI-guided targeted core biopsy of liver and renal tumors at Brigham and Women's Hospital between 2009 and 2012. The intraprocedural MRI scans were acquired on a 3T MRI scanner (MAGNETOM Verio, Siemens Healthcare, Erlangen, Germany) with an 8-channel torso surface coil also known as Body Matrix coil.

T1-weighted fat-suppressed images were acquired using three dimensional (3D) Half Fourier Acquisition Single Shot Turbo Spin Echo (HASTE) sequence (TR/TE: 1000/200 ms; matrix size 320x190, flip angle 147 degree; slice thickness 4 mm; gap 0 mm; field of view 289-340 mm). The MRI datasets were transferred to a computer workstation (Processor: Dual Hexa-Core Intel Xeon 3.06 GHz; random access memory: 6 GB; Fedora 14 operating system) from the hospital's Picture Archiving and Communication System (PACS), using the Digital Image Communication in Medicine (DICOM) and loaded onto 3D Slicer.

On each image, the axis of needle artifact was first identified shown in Fig. 6. This provides a skin entry position and a tangential line was placed on the skin surface to represent the skin contact of the device. By measuring the angle between the lines i.e. device surface line and the axis of needle artifact, needle insertion angle was identified. This result can provide a necessary needle insertion angle that the device should provide. Also, the number of insertion attempt to reach to each biopsy target was measured by counting the number of needle position confirmation scans. Overall procedural time of each biopsy case was obtained from the time stamps between the first scout image and the last confirmation image.

Table 3. Retrospective Clinical Study Results

	Mean	Max	Min	SD
Needle angle (degree)	10.3	26.9	0.4	8.5
Number of attempt	5.3	13.0	2.0	3.9
Procedure Time	15m22s	38m29s	lm34s	12m54s

B. Results

Table 3 shows the tabulated results of the retrospective clinical study. Regarding the needle insertion angle, all biopsy needle insertion angles are within the coverage of the designed insertion angle. In other words, the device could have been used in all the biopsy cases.

The result of the number of needle insertion attempt indicates that on average approximately five needle insertions were performed per target. The additional four needle insertions i.e. the repeat attempts to reach to a satisfactory biopsy position cause not only prolonged procedural time but also additional risk of damaging anatomical features and/or bleeding as well as stress to the clinician.

The overall procedural time is relatively short for the biopsies. The needle guidance device would not save much time. However, if the same needle positioning aid is used in multi target procedure, the effect could be significant, since no repeat attempts are needed for each target when using the device.

V. Phantom Targeting

The proof-of-concept manual device was fabricated from rapid prototyping without post machining. Hence, the accuracy of the needle guidance would be lower and not suitable for quantitative evaluation. Nevertheless, to confirm the kinematic computation of the double ring RCM mechanism and clinical workflow, we conducted a phantom targeting experiment at an image-guided intervention suit that is equipped with a 3T wide-bore MRI scanner (MAGNETOM Verio, Siemens Healthcare, Erlangen, Germany), where the MRI-guided liver interventions take place routinely.

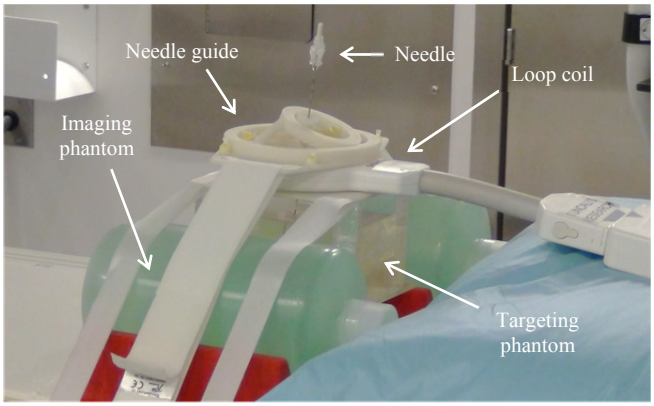

Figure 7. Phantom experiment setup showing the manual needle guidance device, Loop coil, a needle, target phantom srrounded by imaing-aid phantoms.

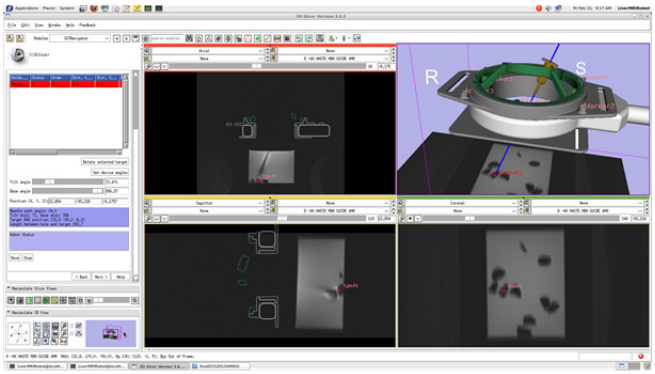

Figure 8. A screenshot of 3D Slicer navigation software during the phantom targeting experiment. The viewing windows are axial, 3D, coronal and saggital view clockwise from top left. The left pane shows required ring orietations and depth to reach a given target.

A custom-made gel phantom that has MR visible targets embedded was used as the target volume and a Loop coil (Siemens Healthcare, Erlangen, Germany) was integrated with device to enhance image quality, which is often used in clinical procedures. Fig. 7 shows the experiment setup.

We followed the clinical MRI sequence that is used in MRI-guided liver interventions. After a scout image, we determined a region of interest, where the registration makers on the device and the embedded targets are all visible. Using HASTE sequence (TR/TE: 1060/200 ms; matrix size 320x272, flip angle 147 degree; slice thickness 4 mm; gap 0 mm; field of view 289-340 mm), images of the device and targets are obtained. This allowed the device registration described in Section III and target identification.

Once the device is registered in the scanner coordinate and a target is selected, the inverse kinematics computes the necessary rotation and tilt angles of the base and small ring as well as the insertion depth. With the given insertion information, the device was manually set to desired angle and a needle was inserted. Fig. 8 shows a screenshot of a confirmation image on the navigation software showing a target position and the needle artifact reached to the target.

We performed a number of needle insertions at various embedded targets and all targeting were achieved by a single needle insertion. Despite the poor precision of the rapid prototype device and the limited manual angling resolution (1 degree for the base ring and 2 degree for the tilted ring), the phantom targeting resulted in less than 6 mm error.

VI. Conclusion and Future Work

We designed a robotic needle guidance device using a double ring RCM mechanism for MRI-guided liver intervention. To evaluate the feasibility, we fabricated a manual guide device prototype and planning/navigation software. A retrospective clinical study showed that the device design is sufficient for clinical cases and the device could radically reduce the number of needle insertion attempt.

Considering that the experiment was conducted in controlled environment e.g. no patient movement by respiratory motion and no needle bending by tissue inhomogeneity, practical targeting outcome can be less accurate. However, this experiment successfully validated the kinematics of the device and the navigation protocol of the 3D Slicer module.

A phantom targeting experiment confirmed that the unique kinematic design was successfully implementation in the targeting. As a next step, we plan to develop a clinically deployable manual needle guidance device while we pursue the ultimate goal of a fully motorized needle insertion device for MRI-guided percutaneous interventions.

References

[1] A. M. Okamura, C. Simone, and M. D. O'Leary, "Force modeling for needle insertion into soft tissue," *IEEE Trans Biomed Eng,* vol. 51, no. 10, pp. 1707-16, Oct, 2004.

[2] K. Masamune, E. Kobayashi, Y. Masutani *et al.*, "Development of an MRI-compatible needle insertion manipulator for stereotactic neurosurgery," *J Image Guid Surg,* vol. 1, no. 4, pp. 242-8, 1995.

[3] F. Wu, M. Torabi, A. Golden *et al.*, "Compact, Patient-Mounted MRI-guided Robot for Accurate Positioning of Multiple Cryoablation Probes," *in Proc. of Fifth National Image Guided Therapy Workshop*, 2012.

[4] J. Tokuda, S. E. Song, G. S. Fischer *et al.*, "Preclinical evaluation of an MRI-compatible pneumatic robot for angulated needle placement in transperineal prostate interventions," *Int J Comput Assist Radiol Surg,* vol. 7, no. 6, pp. 949-57, Nov, 2012.

[5] G. Fischer, I. Iordachita, C. Csoma *et al.*, "Pneumatically operated MRI-compatible needle placement robot for prostate interventions," *in Proc of IEEE International Conference on Robotics and Automation*, 2008.

[6] N. Hata, J. Tokuda, S. Hurwitz *et al.*, "MRI-compatible manipulator with remote-center-of-motion control," *J Magn Reson Imaging,* vol. 27, no. 5, pp. 1130-8, May, 2008.

[7] G. S. Fischer, I. Iordachita, C. Csoma *et al.*, "MRI-Compatible Pneumatic Robot for Transperineal Prostate Needle Placement," *IEEE ASME Trans Mechatron,* vol. 13, no. 3, pp. 295-305, Jun 1, 2008.

[8] H. Elhawary, A. Zivanovic, Z. T. Tse *et al.*, "A magnetic-resonance-compatible limb-positioning device to facilitate magic angle experiments in vivo," *Proc Inst Mech Eng H,* vol. 222, no. 5, pp. 751-60, Jul, 2008.

[9] D. Stoianovici, A. Patriciu, D. Petrisor *et al.*, "A New Type of Motor: Pneumatic Step Motor," *IEEE ASME Trans Mechatron,* vol. 12, no. 1, pp. 98-106, Feb 1, 2007.

[10] H. Su, G. Cole, N. Hata *et al.*, "Real-time MRI-guided Transperineal Needle Placement Prostate Interventions with Piezoelectrically Actuated Robotic Assistance," *Radiological Society of North America 97th Scientific Assembly and Annual Meeting*, 2011.

[11] S. Song, J. Tokuda, K. Tuncali *et al.*, "Development and Preliminary Evaluation of a Motorized Needle Guide Template for MRI-guided Targeted Prostate Biopsy," *IEEE Trans Biomed Eng*, Jan 15, 2013.

[12] T. Suzuki, H. Liao, E. Kobayashi *et al.*, "Ultrasonic motor driving method for EMI-free image in MR image-guided surgical robotic system," *in Proc. IEEE Int. Conf. Intell. Robots Syst. (IROS)*, 2007.

[13] C. Bergeles, P. Vartholomeos, L. Qin *et al.*, "Closed-loop commutation control of an MRI-powered robot actuator," *in press in IEEE Int. Conf. Robotics and Automation*, 2013.

[14] C. Walsh, N. Hanumara, A. Slocum *et al.*, "A Patient-Mounted, Telerobotic Tool for CT-Guided Percutaneous Interventions," *Journal of Medical Devices,* vol. 2, no. 1, pp. 011007-10, 2008.

[15] S. P. DiMaio, E. Samset, G. Fischer *et al.*, "Dynamic MRI scan plane control for passive tracking of instruments and devices," *Med Image Comput Comput Assist Interv,* vol. 10, no. Pt 2, pp. 50-8, 2007.

[16] H. Su, D. Cardona, W. Shang *et al.*, "A MRI-guided concentric tube continuum robot with piezo¬electric actuation: A feasibility study," *IEEE ICRA 2012 International Conference on Robotics and Automation*, 2012.